Water Science and Engineering 2017, 10(4): 275–286

HOSTED BY

ELSEVIER

Available online at www.sciencedirect.com

Water Science and Engineering

journal homepage: http://www.waterjournal.cn

Wave propagation speeds and source term influences in single and integral porosity shallow water equations

Ilhan Özgen [a,*], Jia-heng Zhao [a], Dong-fang Liang [b], Reinhard Hinkelmann [a]

[a] *Department of Civil Engineering, Technische Universität Berlin, Berlin 13355, Germany*
[b] *Department of Engineering, University of Cambridge, Cambridge CB2 1PZ, UK*

Received 26 April 2017; accepted 19 July 2017
Available online 14 December 2017

Abstract

In urban flood modeling, so-called porosity shallow water equations (PSWEs), which conceptually account for unresolved structures, e.g., buildings, are a promising approach to addressing high CPU times associated with state-of-the-art explicit numerical methods. The PSWE can be formulated with a single porosity term, referred to as the single porosity shallow water model (SP model), which accounts for both the reduced storage in the cell and the reduced conveyance, or with two porosity terms: one accounting for the reduced storage in the cell and another accounting for the reduced conveyance. The latter form is referred to as an integral or anisotropic porosity shallow water model (AP model). The aim of this study was to analyze the differences in wave propagation speeds of the SP model and the AP model and the implications of numerical model results. First, augmented Roe-type solutions were used to assess the influence of the source terms appearing in both models. It is shown that different source terms have different influences on the stability of the models. Second, four computational test cases were presented and the numerical models were compared. It is observed in the eigenvalue-based analysis as well as in the computational test cases that the models converge if the conveyance porosity in the AP model is close to the storage porosity. If the porosity values differ significantly, the AP model yields different wave propagation speeds and numerical fluxes from those of the BP model. In this study, the ratio between the conveyance and storage porosities was determined to be the most significant parameter.

Keywords: Porosity; Macroscopic modeling of urban flooding; Wave propagation speed; Godunov flux; Single porosity shallow water model; Anisotropic porosity shallow water model

1. Introduction

Urban flooding is a multiscale process. An urban catchment might span several hundreds of square kilometers, and individual buildings usually span up to a hundred square meters. The interaction between individual buildings or building blocks and the flood wave, occurring at the building scale, is the most significant process influencing the entire flow field.

Using a two-dimensional shallow water model, or a simplified form of it, to model urban flooding is considered the state-of-the-art methodology. In classical shallow water models, buildings have to be explicitly discretized either by increasing the bed elevation accordingly or by removing the corresponding areas from the computational mesh (Schubert and Sanders, 2012). In both cases, the mesh has to be locally refined near the buildings, which results in high numbers of cells. In recent years, explicit Godunov-type methods have attracted increasing interest as applied to such tasks, because of their attractive numerical properties (shock-capturing, monotonicity preserving, and the ability to deal with wet/dry fronts and transcritical flow). The high computational cost of these types of methods, combined with high numbers of cells leads to a huge CPU requirement that is classically approached by means of parallel computation techniques (Hinkelmann, 2005).

* Corresponding author.
E-mail address: ilhan.oezgen@wahyd.tu-berlin.de (Ilhan Özgen).
Peer review under responsibility of Hohai University.

https://doi.org/10.1016/j.wse.2017.12.003

The so-called macroscopic modeling of urban floods is an alternative approach, in which the catchment is discretized using a coarser resolution than the building scale, i.e., the size of the cell is larger than that of the building, and conceptual approaches are used to describe certain hydraulic properties of the urban catchment. Typically, porosity terms are used to account for the presence of buildings inside a computational cell without explicitly discretizing them. These equations are then referred to as porosity shallow water equations (PSWEs). Inspired by the pioneering work in Defina (2000), Guinot and Soares-Frazão (2006) derived the single porosity shallow water model (SP model), which uses a single porosity defined inside the cell to account for reductions in storage and conveyance. Sanders et al. (2008) derived an integral porosity model, also referred to as the anisotropic porosity shallow water model (AP model), where the storage reduction is accounted for with a porosity term defined inside the cell and the conveyance reduction is accounted for with a porosity term at the cell edges. In Özgen et al. (2016a, 2016b), water depth-dependent porosities were derived to enable full inundation of sub-grid elements.

Guinot and Soares-Frazão (2006) as well as Mohamed (2014) have shown that the wave propagation speeds of the SP model are the same as those of the classical shallow water equations. As shown in Guinot et al. (2017), the wave propagation speeds of the AP model differ from those of the classical shallow water equations and the SP model, and these findings are supported by numerical experiments conducted in Özgen et al. (2016b). In addition, different source terms arise in the SP model and the AP model. Recently, Ferrari et al. (2017) derived an augmented Roe scheme for the SP model that incorporates the source term in the Riemann problem.

In this study, the implications of the differences in wave propagation speeds and source terms between the SP model and the AP model were analyzed, using a methodology described in Murillo et al. (2007). The governing equations of the SP model and the AP model are presented, accompanied by an eigenvalue analysis for each mathematical model. Then, the influences of the wave propagation speeds and the source terms on the stability of each model are analyzed. Finally, computational tests for investigation of the influences of the wave propagation speeds and source terms on the model results are described.

2. Governing equations

2.1. Single porosity shallow water equation

The single PSWE, i.e., the SP model, is written in the vector form as follows:

$$\frac{\partial}{\partial t}(\phi \boldsymbol{q}) + \frac{\partial}{\partial x}(\phi \boldsymbol{f}) + \frac{\partial}{\partial y}(\phi \boldsymbol{g}) = \phi \boldsymbol{s}_{\Omega} + \boldsymbol{s}_{\phi} \tag{1}$$

where t is time; x and y are the axes in the Cartesian coordinate system; ϕ is the storage porosity expressing the fraction of the control volume that is not occupied by structures; $\boldsymbol{q}$ is the vector of conserved variables; $\boldsymbol{f}$ and $\boldsymbol{g}$ are the flux vectors in the x- and y-directions, respectively; $\boldsymbol{s}_{\Omega}$ is the source term in the control volume; and $\boldsymbol{s}_{\phi}$ is the porosity source term that describes the momentum variation due to the variation in porosity. The vectors are defined as follows:

$$\boldsymbol{q} = \begin{bmatrix} h \\ uh \\ vh \end{bmatrix} \tag{2}$$

$$\boldsymbol{f} = \begin{bmatrix} uh \\ hu^2 + \frac{g}{2}h^2 \\ uvh \end{bmatrix} \qquad \boldsymbol{g} = \begin{bmatrix} uh \\ uvh \\ hv^2 + \frac{g}{2}h^2 \end{bmatrix} \tag{3}$$

$$\boldsymbol{s}_{\Omega} = \begin{bmatrix} 0 \\ s_{gx} + s_{fx} \\ s_{gy} + s_{fy} \end{bmatrix} \qquad \boldsymbol{s}_{\phi} = \begin{bmatrix} 0 \\ g\frac{h^2}{2}\frac{\partial \phi}{\partial x} \\ g\frac{h^2}{2}\frac{\partial \phi}{\partial y} \end{bmatrix} \tag{4}$$

where h is the water depth; u and v are the velocities in the x- and y-directions, respectively; g is the acceleration due to gravity; s_{gx} and s_{gy} are the geometric source terms in the x- and y-directions, respectively; and s_{fx} and s_{fy} are the friction source terms in the x- and y-directions, respectively.

The source term $\boldsymbol{s}_{\Omega}$ describes two separate processes: the momentum variation due to the gravity, which can be calculated as follows:

$$s_{gx} = -gh\frac{\partial z}{\partial x} \qquad s_{gy} = -gh\frac{\partial z}{\partial y} \tag{5}$$

where z is the bed elevation; and the momentum variation due to friction and drag, which can be calculated using Manning's law:

$$s_{fx} = -\left(c_D^f + c_D^b\right)\|\boldsymbol{v}\|u \qquad s_{fy} = -\left(c_D^f + c_D^b\right)\|\boldsymbol{v}\|v \tag{6}$$

where c_D^f is the drag coefficient due to bottom friction, c_D^b is the drag coefficient due to buildings, $\boldsymbol{v}$ is the velocity vector, and $\|\boldsymbol{v}\|$ denotes the L_2-norm of the vector $\boldsymbol{v}$. c_D^f can be calculated by means of classical friction laws such as Manning's law. Many drag laws have been proposed in the literature, ranging from empirical equations for head loss at sudden contractions (Soares-Frazão et al., 2008) to equations inspired by vegetation-induced drag laws (Nepf, 1999; Sanders et al., 2008).

The derivation of Eq. (1) through (4), initially presented in Guinot and Soares-Frazão (2006), is based on homogenizing heterogeneities inside a control volume, expressed with a single variable ϕ, which implies the assumption of a representative elementary volume (REV). As discussed in Guinot (2012), the existence of such an REV in the urban area is controversial but has no consequences with regard to the applicability of the equations.

An eigenvalue analysis of the homogeneous, one-dimensional version of Eq. (1), i.e.,

$$\frac{\partial}{\partial t}(\phi \boldsymbol{q}) + \frac{\partial}{\partial x}(\phi \boldsymbol{f}) = 0 \tag{7}$$

is presented in Mohamed (2014) and Guinot et al. (2017). Eq. (7) is linearized as follows:

$$\frac{\partial}{\partial t}(\phi \boldsymbol{q}) + \boldsymbol{A}\frac{\partial}{\partial x}(\phi \boldsymbol{q}) = 0 \tag{8}$$

where $\boldsymbol{A}$ is the Jacobian matrix, which is calculated as follows:

$$\boldsymbol{A} = \frac{\partial \boldsymbol{f}}{\partial \boldsymbol{q}} = \begin{bmatrix} 0 & 1 & 0 \\ c^2 - u^2 & 2u & 0 \\ -uv & v & u \end{bmatrix} \tag{9}$$

with c being the wave celerity, and

$$c = \sqrt{gh} \tag{10}$$

The real and distinct eigenvalues of Eq. (7) are then determined to be

$$\lambda_1 = u - c \qquad \lambda_2 = u \qquad \lambda_3 = u + c \tag{11}$$

which are the same as those of the classical shallow water equations (LeVeque, 2002). Consequently, the right eigenvectors of Eq. (1) are also identical to those of the classical shallow water equations:

$$\boldsymbol{r}_1 = \begin{bmatrix} 1 \\ u - c \\ v \end{bmatrix} \qquad \boldsymbol{r}_2 = \begin{bmatrix} 0 \\ 0 \\ 1 \end{bmatrix} \qquad \boldsymbol{r}_3 = \begin{bmatrix} 1 \\ u + c \\ v \end{bmatrix} \tag{12}$$

In Mohamed (2014), Eq. (1) was augmented with an additional equation:

$$\frac{\partial \phi}{\partial t} = 0 \tag{13}$$

which yields the fourth eigenvalue, $\lambda_4 = 0$, for a stationary wave, associated with the variable ϕ.

2.2. Integral porosity shallow water equation

The limitation of the SP model is its inability to represent directionality and blocking effects (Guinot, 2012). In order to overcome this limitation, an integral form of PSWEs was presented in Sanders et al. (2008), which uses a storage porosity defined inside the control volume to account for the reduction in storage and a conveyance porosity defined at the edge of the control volume to account for the reduction in conveyance. In the literature, these equations are referred to as the anisotropic or integral PSWEs.

As these equations are in the integral form, discontinuous solutions are allowed and there is no need for an REV assumption for the derivation. Porosities are calculated by means of a phase function $\varphi(x,y)$ that is 1 if the evaluation point (x,y) corresponds to a void and 0 if it corresponds to an obstacle. Then, the storage porosity is calculated as follows:

$$\phi = \frac{1}{\Omega}\int_{\Omega} \varphi \mathrm{d}\Omega \tag{14}$$

and the conveyance porosity is calculated as follows:

$$\psi = \frac{1}{\Gamma}\oint_{\Gamma} \varphi \mathrm{d}\Gamma \tag{15}$$

with Ω being the control volume, and Γ being the boundary of the control volume.

The AP model is written in the vector form as follows:

$$\frac{\partial}{\partial t}\int_{\Omega} \varphi \boldsymbol{q}\mathrm{d}\Omega + \oint_{\Gamma} \varphi \boldsymbol{F}\cdot\boldsymbol{n}\mathrm{d}\Gamma = \frac{\partial}{\partial t}\int_{\Omega} \varphi \boldsymbol{s}_{\Omega}\mathrm{d}\Omega + \oint_{\Gamma} \varphi \boldsymbol{s}_{\Gamma}\cdot\boldsymbol{n}\mathrm{d}\Gamma \tag{16}$$

with $\boldsymbol{F}$ being the flux tensor, $\boldsymbol{n}$ being the unit normal vector pointing outwards from the control volume, and $\boldsymbol{s}_{\Gamma}$ being the source term at the boundary, which arises due to unresolved solid-fluid interface pressures (Bird et al., 2007). $\boldsymbol{q}$ and $\boldsymbol{s}_{\Omega}$ are defined in Eqs. (2) and (4), and $\boldsymbol{F}$ and $\boldsymbol{s}_{\Gamma}$ are written as follows:

$$\boldsymbol{F} = \begin{bmatrix} uh & vh \\ hu^2 + \frac{g}{2}h^2 & uvh \\ uvh & hv^2 + \frac{g}{2}h^2 \end{bmatrix} \qquad \boldsymbol{s}_{\Gamma} = \begin{bmatrix} 0 & 0 \\ \frac{g}{2}h_{\eta_0}^2 & 0 \\ 0 & \frac{g}{2}h_{\eta_0}^2 \end{bmatrix} \tag{17}$$

where h_{η_0} represents the water depth inside the cell, evaluated for a constant average water level elevation η_0 inside the control volume. Carrying out discretized integral of the individual terms in Eq. (16) and using Eqs. (14) and (15) provide the following:

$$\frac{\partial}{\partial t}(\phi \boldsymbol{q}) + \sum_j (\psi \boldsymbol{F}\cdot\boldsymbol{n})_j l_j = \boldsymbol{s} \tag{18}$$

where l_j is the length of the jth boundary edge, and $\boldsymbol{s}$ stands for a suitable integration of the source terms $\boldsymbol{s}_{\Omega}$ and $\boldsymbol{s}_{\Gamma}$. The integral over the boundary in Eq. (16) has been replaced by a sum over j discrete boundary edges. Eq. (18) is essentially a finite volume discretization, and indeed, because Eq. (16) is only meaningful in the integral form, it can only be solved by means of a finite volume method.

Going back to Eq. (16), under the assumption that the solution is sufficiently smooth, the control volume can be made infinitesimally small. Applying the Green-Gauß theorem yields the differential form of the AP model. This technique has been applied in Sanders et al. (2008), where it is shown that in the context of an infinitesimally small control volume, the storage porosity ϕ equals the conveyance porosity ψ, and the AP model is made equivalent to the SP model. Based on the discussion in Guinot et al. (2017), for the sake of argument, the porosity terms are not set to be equal, which then,

after algebraic manipulation, leads to the following differential form of the AP model:

$$\frac{\partial}{\partial t}(\phi \boldsymbol{q}) + \frac{\partial}{\partial x}(\psi \boldsymbol{f}) + \frac{\partial}{\partial y}(\psi \boldsymbol{g}) = \phi \boldsymbol{s}_{\Omega} + \frac{\partial}{\partial x}(\psi \boldsymbol{s}_{\Gamma x}) + \frac{\partial}{\partial y}(\psi \boldsymbol{s}_{\Gamma y}) \tag{19}$$

where $\boldsymbol{f}$ and $\boldsymbol{g}$ are identical to the flux vectors in Eq. (1), and $\boldsymbol{s}_{\Omega}$ is identical to the source term presented in Eq. (4). The boundary source terms $\boldsymbol{s}_{\Gamma x}$ and $\boldsymbol{s}_{\Gamma y}$ are the first and second columns of $\boldsymbol{s}_{\Gamma}$ and replace the source term $\boldsymbol{s}_{\phi}$ in Eq. (1).

It is perhaps interesting to note that a source term similar to $\boldsymbol{s}_{\phi}$ appears in the cross-section-averaged Saint-Venant equations due to channel narrowing, which, through Leibniz's rule for differentiation under the integral sign, can be transformed into a form similar to $\boldsymbol{s}_{\Gamma}$ (Cunge et al., 1980).

Considering again only the homogeneous part of the one-dimensional form of Eq. (19), i.e.,

$$\frac{\partial}{\partial t}(\phi \boldsymbol{q}) + \frac{\partial}{\partial x}(\psi \boldsymbol{f}) = 0 \tag{20}$$

and linearizing Eq. (20) provide the following:

$$\frac{\partial}{\partial t}(\phi \boldsymbol{q}) + \boldsymbol{B}\frac{\partial}{\partial x}(\phi \boldsymbol{q}) = 0 \tag{21}$$

with the Jacobian matrix $\boldsymbol{B}$ defined as

$$\boldsymbol{B} = \frac{\partial(\psi \boldsymbol{f})}{\partial(\phi \boldsymbol{q})} = \frac{\psi}{\phi}\boldsymbol{A} \tag{22}$$

The real and distinct eigenvalues of Eq. (20) are calculated as

$$\lambda_1 = \frac{\psi}{\phi}(u - c) \qquad \lambda_2 = \frac{\psi}{\phi}u \qquad \lambda_3 = \frac{\psi}{\phi}(u + c) \tag{23}$$

which differ from those in the SP model (Eq. (11)) by the factor ψ/ϕ. Guinot et al. (2017) note that if $\psi/\phi > 1$, the wave propagation speeds of the AP model are larger than those of the classical shallow water model. This would imply that the presence of the conveyance porosity increases the wave propagation speed, which is physically not meaningful. The right eigenvectors of Eq. (19) are obtained, which are the same as Eq. (12).

2.3. Comparison of source term influences in first-order upwind scheme

Both the SP model and the AP model are hyperbolic systems. The wave propagation speeds are equal to the eigenvalues of the system, and, therefore, by comparing Eq. (23) with Eq. (11), it is clear that wave propagation speeds of the AP model differ from those of the SP model by the factor ψ/ϕ. Therefore, in cases where the ratio ψ/ϕ deviates from 1, different model behaviors are expected.

It is noted that the wave propagation speeds were calculated for the homogeneous system in this study, yet both models have different porosity source terms. Specifically, the SP model has the porosity gradient source term $\boldsymbol{s}_{\phi}$ (Eq. (1)), and the AP model has the solid-fluid interface pressure source term $\boldsymbol{s}_{\Gamma}$ in the x- and y-directions (Eq. (19)). These source terms are expected to have different influences on the model results.

2.3.1. Roe-type solutions by Murillo et al. (2007) to study influence of source terms

In this section, Roe-type solutions introduced in Murillo et al. (2007) are briefly presented and then used to assess the influence of source terms in both models for an explicit first-order upwind scheme.

Consider a computational cell i with N edges in a finite-volume framework for solving a hyperbolic system that generates three waves. A first-order upwind scheme can be written in the so-called wave propagation form (LeVeque, 2002) by projecting the variations of the flux vector and source term across the cell edge based on the eigenvector of the homogeneous system:

$$\boldsymbol{q}_i^{n+1} = \boldsymbol{q}_i^{n} - \sum_{k=1}^{N}\sum_{m=1}^{3}\left[\left(\lambda^{-}\delta w - \delta b^{-}\right)\boldsymbol{r}\right]_k^m l_k \frac{\Delta t}{A_i} \tag{24}$$

where $\boldsymbol{q}_i^n$ is the vector of conserved variables for cell i at the nth time step; m is the wave number, such that λ^{-m} is the speed of the ingoing m-wave, $\boldsymbol{r}^m$ is the right eigenvector corresponding to the m-wave, and δw^m and δb^{-m} denote the m-wave components of $\delta \boldsymbol{w}$ and $\delta \boldsymbol{b}^{-}$, respectively; k means the cell edge k, such that l_k is the length of the cell edge k; and A_i is the area of cell i. $\delta \boldsymbol{w}$ is the variation of the wave strength vector $\boldsymbol{w}$ across the cell edge, which can be calculated as follows:

$$\delta \boldsymbol{w} = \boldsymbol{R}^{-1}\delta \boldsymbol{q} \tag{25}$$

where $\delta \boldsymbol{q}$ is the variation of $\boldsymbol{q}$ across the cell edge, and $\boldsymbol{R}^{-1}$ is the inverse matrix of $\boldsymbol{R}$ that is composed of the right eigenvectors as column vectors. $\delta \boldsymbol{b}^{-}$ denotes the ingoing contribution of the source term, with $\delta \boldsymbol{b}$ being the variation of the source term strength vector across the cell edge, which is calculated as follows:

$$\delta \boldsymbol{b} = \boldsymbol{R}^{-1}\delta \boldsymbol{s} \tag{26}$$

where $\delta \boldsymbol{s}$ denotes the variation of the source term across the cell edge. Eq. (24) can be rewritten as follows:

$$\boldsymbol{q}_i^{n+1} = \boldsymbol{q}_i^{n} - \sum_{k=1}^{N}\sum_{m=1}^{3}\left(\theta\lambda^{-}\delta w\boldsymbol{r}\right)_k^m l_k \frac{\Delta t}{A_i} \tag{27}$$

with

$$\theta_k^m = 1 - \left(\frac{\delta b^{-}}{\lambda^{-}\delta w}\right)_k^m \tag{28}$$

Murillo et al. (2007) show that monotonicity of the conserved variables in the presence of source terms requires the following:

$$\left(\theta\lambda^{-}\right)_k^m \le 0 \qquad \theta_k^m \ge 0 \qquad \forall m \tag{29}$$

The Courant-Friedrichs-Lewy (CFL) condition restricts the time step of the explicit scheme as follows:

$$\Delta t = C\Delta t_{\max} \tag{30}$$

where C is the CFL number, and $C \le 1$; and $\Delta t_{\max}$ is calculated as follows:

$$\Delta t_{\max} = \min \Delta t_k \qquad \Delta t_k = \frac{A_k}{\max\left(\theta\lambda^{-}\right)_k^m l_k} \tag{31}$$

where A_k is the minimum of the areas of the cells located at the left and right sides of the cell edge k. For $\theta_k^m = 1$, Eq. (31) is identical to the stability condition for homogeneous systems. For $0 < \theta_k^m < 1$, the stability region of the numerical scheme enlarges, i.e., larger time steps are allowed, as the source term acts opposite to the flux term. For $\theta_k^m < 0$, the source term dominates the flux term, and the stability region has to be redefined by calculating Δt_k as follows:

$$\Delta t_k = \gamma \frac{A_k}{\max\left(\theta\lambda^{-}\right)_k^m l_k} \tag{32}$$

where γ is calculated depending on the constraints of the physical problem, and $0 \le \gamma \le 1$.

2.3.2. Application of Roe-type solutions to SP model

In the SP model, $\boldsymbol{R}$ and $\boldsymbol{R}^{-1}$ can be calculated as follows:

$$\boldsymbol{R} = \begin{bmatrix} 1 & 0 & 1 \\ u-c & 0 & u+c \\ v & 1 & v \end{bmatrix} \qquad \boldsymbol{R}^{-1} = \begin{bmatrix} \dfrac{c+u}{2c} & -\dfrac{1}{2c} & 0 \\ -v & 0 & 1 \\ \dfrac{c-u}{2c} & \dfrac{1}{2c} & 0 \end{bmatrix} \tag{33}$$

Using Eq. (25), $\delta\boldsymbol{w}$ is calculated as follows:

$$\delta\boldsymbol{w}_k = \begin{bmatrix} \dfrac{\delta q_1(\tilde{c}+\tilde{u})}{2\tilde{c}} - \dfrac{\delta q_2}{2\tilde{c}} \\ \delta q_3 - \delta q_1 \tilde{v} \\ \dfrac{\delta q_2}{2\tilde{c}} - \dfrac{\delta q_1(\tilde{u}-\tilde{c})}{2\tilde{c}} \end{bmatrix}_k = \begin{bmatrix} \dfrac{\delta(\phi h)(\tilde{c}+\tilde{u})}{2\tilde{c}} - \dfrac{\delta(\phi h u)}{2\tilde{c}} \\ \delta(\phi h v) - \tilde{v}\delta(\phi h) \\ \dfrac{\delta(\phi h u)}{2\tilde{c}} - \dfrac{\delta(\phi h)(\tilde{u}-\tilde{c})}{2\tilde{c}} \end{bmatrix}_k \tag{34}$$

where the tilde denotes that the values are obtained for an intermediate state, e.g., using Roe-averaged values; δ denotes the variation of a value across the cell edge; and q_1, q_2, and q_3 are the first, second, and third components of $\boldsymbol{q}$, respectively.

Using Eq. (26), $\delta\boldsymbol{b}$ is obtained as follows:

$$\delta\boldsymbol{b}_k = \begin{bmatrix} -\dfrac{\delta s_2}{2\tilde{c}} \\ 0 \\ \dfrac{\delta s_2}{2\tilde{c}} \end{bmatrix}_k \tag{35}$$

where s_2 is the second component of the source term $\boldsymbol{s}$ obtained with a suitable numerical discretization. For demonstration purposes, the following discretization is chosen for calculation of δs_2:

$$\delta s_2 = \frac{1}{2} g \overline{h}^2 \delta\phi \tag{36}$$

where $\overline{h}$ is the average of the water depths at the left and right sides of the cell edge k. Using Eq. (28), θ_k^m can be determined as follows:

$$\begin{cases} \theta_k^1 = 1 + \left\{ \dfrac{1}{2} \dfrac{g\overline{h}^2 \delta\phi}{(\tilde{u}-\tilde{c})[\delta(\phi h)(\tilde{c}+\tilde{u}) - \delta(\phi h u)]} \right\}_k \\ \theta_k^2 = 1 \\ \theta_k^3 = 1 - \left\{ \dfrac{1}{2} \dfrac{g\overline{h}^2 \delta\phi}{(\tilde{u}+\tilde{c})[\delta(\phi h u) - \delta(\phi h)(\tilde{u}-\tilde{c})]} \right\}_k \end{cases} \tag{37}$$

2.3.3. Application of Roe-type solutions to AP model

The matrices $\boldsymbol{R}$ and $\boldsymbol{R}^{-1}$ of the AP model are identical to those in Eq. (33). However, because the porosity ψ defined at the cell edge is different from the porosity ϕ inside the cell in the AP model, variables have to be reconstructed at the edge. Sanders et al. (2008) noted that, for the reconstruction of velocities, $\phi u h$ and $\phi v h$ should be used, as they are the conserved variables. The variables are reconstructed for first-order accuracy as follows:

$$h_k = h_i \qquad u_k = \frac{(\phi u h)_i}{(\psi h)_k} \qquad v_k = \frac{(\phi v h)_i}{(\psi h)_k} \tag{38}$$

The subscript i implies that values are at the center of cell i, and the subscript k implies that values are at the cell edge k. This can be simplified as follows:

$$h_k = h_i \qquad u_k = \frac{\phi_i}{\psi_k} u_i \qquad v_k = \frac{\phi_i}{\psi_k} v_i \tag{39}$$

It is noted that, because ϕ_i is always larger than or equal to ψ_k, according to Eq. (39), the reconstructed velocities at the edge will always be larger than or equal to the velocities in the cell. The upwind scheme in the wave propagation form is written as

$$\boldsymbol{q}_i^{n+1} = \boldsymbol{q}_i^n - \sum_{k=1}^{N} \sum_{m=1}^{3} \left(\theta\lambda^{-}\delta w \boldsymbol{r}\right)_k^m l_k \frac{\Delta t}{A_i} - \sum_{k=1}^{N} \sum_{m=1}^{3} \left(\theta\lambda^{-}\delta w \boldsymbol{r}\right)_0^m l_k \frac{\Delta t}{A_i} \tag{40}$$

In addition to the waves induced by the variations of the flux vector and source term across the cell edge, additional waves appear due to the differences in the flux vector and source term at the cell center and cell edge, which yield the third term in Eq. (40), described with the subscript 0. Using Eq. (28), θ_k^m and θ_0^m can be calculated, with the major difference being that, in the calculation of θ_0^m, differences between values of $\delta\boldsymbol{w}$ and $\delta\boldsymbol{b}$ at the cell center and cell edge are

considered, rather than the variations of values across the cell edge.

The monotonicity is ensured when $\theta_k^m \geq 0$ and $\theta_0^m \geq 0$. The stability region is defined as the set of time steps satisfying Eq. (30), with $C \leq 1/3$, and $\Delta t_{\max}$ is calculated as follows:

$$\Delta t_{\max} = \min \Delta t_k \qquad \Delta t_k = \frac{A_k}{\max\left(\theta_k \lambda_k^-, \theta_0 \lambda_0\right)^m l_k} \tag{41}$$

Then, the stability region enlarges when $0 \leq \theta_k^m \leq 1$ and $0 \leq \theta_0^m \leq 1$. For negative values of θ_k^m or θ_0^m, the source term dominates. In Murillo et al. (2007), it is noted that, in this case, the reconstruction of variables should fall back to first-order accuracy. However, in the AP model, this is not possible, as the reconstructed results are not the product of a higher-order extrapolation but inherent to the mathematical model. The optimal treatment in these situations has to be addressed in future research.

$\delta \boldsymbol{w}$ and $\delta \boldsymbol{b}$ are calculated using Eq. (25) and Eq. (26), respectively, as follows:

$$\delta \boldsymbol{w}_k = \begin{bmatrix} \dfrac{\delta(\phi h)(\tilde{c}+\tilde{u})}{2\tilde{c}} - \dfrac{\delta\left[\left(\phi^2/\psi\right)hu\right]}{2\tilde{c}} \\ \delta\left[\left(\phi^2/\psi\right)hv\right] - \tilde{v}\delta(\phi h) \\ \dfrac{\delta\left[\left(\phi^2/\psi\right)hu\right]}{2\tilde{c}} - \dfrac{\delta(\phi h)(\tilde{u}-\tilde{c})}{2\tilde{c}} \end{bmatrix}_k \qquad \delta \boldsymbol{b}_k = \begin{bmatrix} -\dfrac{\delta s_2}{2\tilde{c}} \\ 0 \\ \dfrac{\delta s_2}{2\tilde{c}} \end{bmatrix}_k \tag{42}$$

$$\delta \boldsymbol{w}_0 = \frac{1}{2\tilde{c}} \begin{bmatrix} -\dfrac{\phi(\phi-\psi)}{\psi} hu \\ -\dfrac{\phi(\phi-\psi)}{\psi} hv \\ \dfrac{\phi(\phi-\psi)}{\psi} hu \end{bmatrix}_0 \qquad \delta \boldsymbol{b}_0 = \begin{bmatrix} -\dfrac{\delta s_2}{2\tilde{c}} \\ 0 \\ \dfrac{\delta s_2}{2\tilde{c}} \end{bmatrix}_0 \tag{43}$$

where δs_2 is calculated as follows:

$$\delta s_2 = \frac{1}{2} g \psi \delta h_{\eta_0}^2 \tag{44}$$

with h_{η_0} to be determined. Then, using Eq. (28), θ_k^m and θ_0^m can be determined as follows:

$$\begin{cases} \theta_k^1 = 1 + \left\{ \dfrac{1}{2} \dfrac{g\phi\delta h_{\eta_0}^2}{(\tilde{u}-\tilde{c})\left\{\delta(\phi h)(\tilde{c}+\tilde{u}) - \delta\left[\left(\phi^2/\psi\right)hu\right]\right\}} \right\}_k \\ \theta_k^2 = 1 \\ \theta_k^3 = 1 - \left\{ \dfrac{1}{2} \dfrac{g\phi\delta h_{\eta_0}^2}{(\tilde{u}+\tilde{c})\left\{\delta\left[\left(\phi^2/\psi\right)hu\right] - \delta(\phi h)(\tilde{u}-\tilde{c})\right\}} \right\}_k \end{cases} \tag{45}$$

$$\begin{cases} \theta_0^1 = 1 + \left[\dfrac{\delta s_2}{(\tilde{u}-\tilde{c})(\phi-\psi)hu} \right]_0 \\ \theta_0^2 = 1 \\ \theta_0^3 = 1 - \left[\dfrac{\delta s_2}{(\tilde{u}+\tilde{c})(\phi-\psi)hu} \right]_0 \end{cases} \tag{46}$$

As δs_2 depends on the slope of h_{η_0}, which is constant inside the cell, the second term in the expressions of θ_0^1 and θ_0^3 in Eq. (46) vanishes in this case, with $\theta_0^1 = \theta_0^2 = \theta_0^3$. This is not true when the variation of h_{η_0} across the cell edge is considered.

It is worth noting that the ratio ϕ^2/ψ also appears in the momentum flux terms of the porosity shallow water model in Guinot et al. (2017) as well and is a direct result of the assumption that ϕuh and ϕvh are conserved between the cell center and edge, i.e., the continuity is preserved. Guinot et al. (2017) used this relationship to derive an improved version of the AP model, the so-called double integral porosity model.

2.3.4. Discussion

The difference between the SP model and the AP model can be studied by comparing Eq. (37) with Eq. (45) for the same Riemann problem. First, it is assumed that both source term contributions are the same, i.e., $g\psi\delta h_{\eta_0}^2 = g\overline{h}^2\delta\phi$. Direct comparison shows that the only difference is that, in the AP model, $\delta(uh)$ is multiplied by the ratio ϕ^2/ψ instead of ϕ.

Now the source term contributions are not assumed to be equal anymore, and θ_k^m in both models is examined in more detail. Given that, for both models, the right eigenvectors are the same as those in the classical shallow water model, it can be assumed that Roe-averaged values give a sufficient approximation of the middle state for both models (Roe, 1981). The conveyance porosity in the AP model is calculated as the minimum of the storage porosity at the left and right sides of the cell edge. Then, θ_k^m can be evaluated for different porosity configurations.

Three different Riemann problems with different initial states were studied, in which h_L, u_L, and ϕ_L were the initial water depth, velocity, and porosity, respectively, constituting the left set of initial values, and h_R, u_R, and ϕ_R were the initial water depth, velocity, and porosity, respectively, constituting the right set of initial values, for the Riemann problem. In case 1, the initial states were defined as $h_L = 10$ m, $h_R = 1$ m, $u_L = 1$ m/s, and $u_R = 0.5$ m/s. In case 2, the left- and right-side water depths were switched (velocities remained the same). In case 3, the left-side water depth was set equal to the right-side water depth (velocities remained the same).

Fig. 1 shows the evaluation of θ_k^1, where the region with $0 \leq \theta_k^1 \leq 1$ is colored grey and referred to as the stability-enhancing region. The evaluation of the SP model is shown in Fig. 1(a), (b), and (c), where $\phi_L = \phi_R$ means that $\theta_k^1 = 1$. It is seen that the stability-enhancing region is mirrored over the line $\phi_L = \phi_R$ in case 1 and case 2 (Fig. 1(a) and (b)). The largest stability-enhancing region is obtained with equal water depths (Fig. 1(c)). In this case, if the values of ϕ_L and ϕ_R are close to each other with $\phi_L > \phi_R$, θ_k^1 leaves the stability-

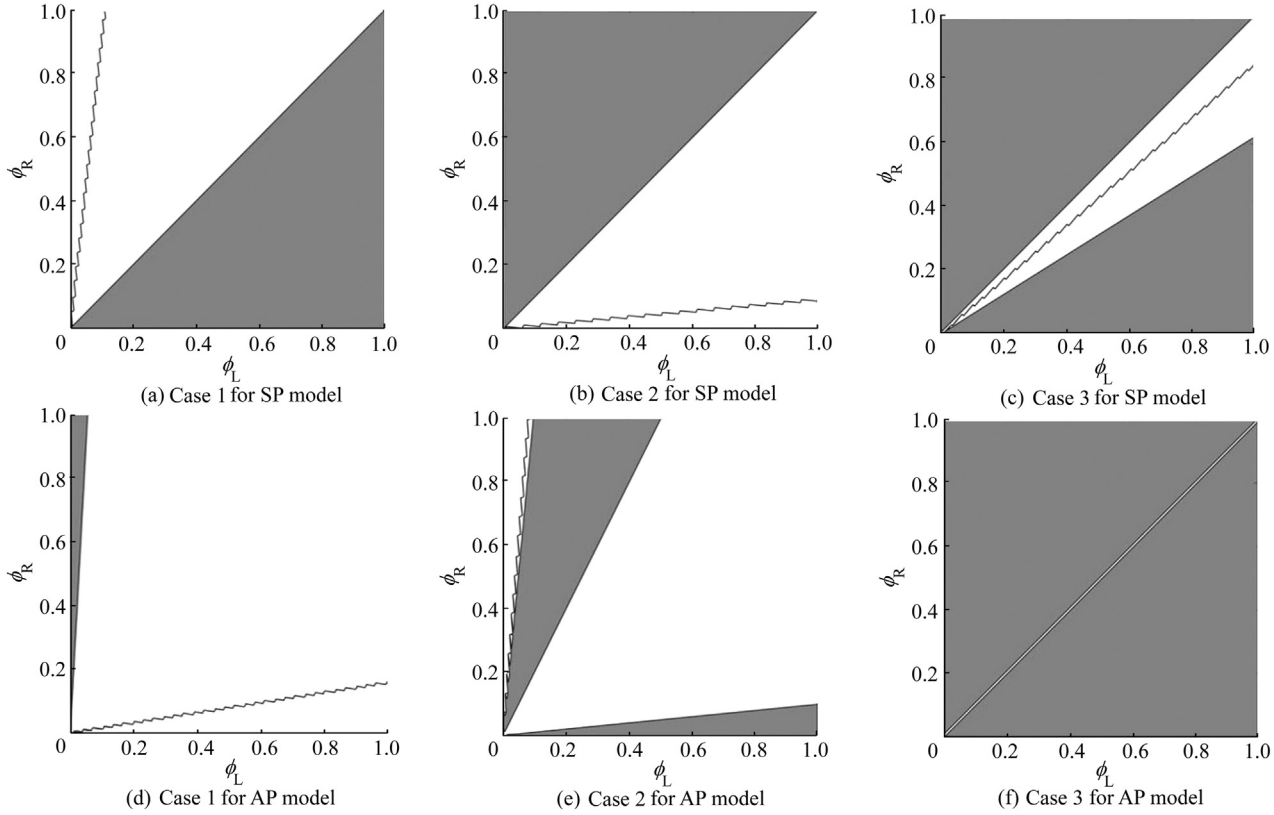

Fig. 1. θ_k^1 for different porosity and water depth configurations in different cases for SP model and AP model.

enhancing region. The stability-reducing region is not symmetric due to the initial velocities.

Fig. 1(d), (e), and (f) show the evaluation of θ_k^1 for the AP model. It is seen that the stability-enhancing region is more sensitive to water depths. This is because the source term is directly related to the water depth variation across the cell edge (Eq. (44)). Consequently, if $h_L = h_R$, the stability-enhancing region comprises all porosity configurations, as the source term vanishes; if the water depths are not equal, the size of the stability-enhancing region is reduced significantly, compared with the SP model. Very similar observations can be made for θ_k^3. For sake of brevity, this discussion is omitted here.

Issues related to the maximum allowable time step are more complicated. The CFL number C for the AP model is not allowed to exceed 1/3, while C for the SP model is allowed to take values up to 1. In addition, due to the required reconstruction of variables in the AP model, additional waves emerge and must be taken into consideration when the time step is calculated (Eq. (41)). It might be concluded that the time steps of the AP model are more severely restricted. However, at the same time, the wave propagation speeds of the AP model are always smaller than those of the SP model, comparing Eq. (23) to Eq. (11).

Neglecting the source terms, Sanders et al. (2008) provided a stability condition for the AP model based on the homogeneous system as follows:

$$\max(\psi_k \lambda_k l_k)\frac{\Delta t}{\phi_i A_i} \leq 1 \tag{47}$$

while Guinot and Soares-Frazão (2006) showed that for the homogeneous system the stability condition of the SP model is

$$\max(\lambda_k l_k)\frac{\Delta t}{A_i} \leq 1 \tag{48}$$

which leads to the same conclusions, i.e., as the wave propagation speeds of the AP model decrease, larger time steps might be allowed. In the authors' experience, the time step of the AP model tends to be smaller compared to that of the SP model in most cases.

3. Computational test cases

Both equations were solved using a first-order Godunov-type finite volume scheme with explicit time integration. The numerical scheme of the SP model was presented in Guinot and Soares-Frazão (2006) and is a so-called *lateralized* scheme, where the influence of the source terms was considered a correction term to the numerical flux. A specialized porous Harten, Lax, and van Leer (HLL) approximate Riemann solver was used for the numerical flux calculation.

The numerical scheme of the AP model calculated the numerical flux through an HLL solver with simplified wave

speed estimates. The discretization of the source terms with the C-property preserved, presented in Özgen et al. (2016a), was used.

3.1. One-dimensional dam break with variable porosity

This test case was initially presented in Guinot and Soares-Frazão (2006) and featured a one-dimensional dam break in a domain with variable porosity. The domain was 100 m long and the dam was placed at $x = 50$ m. At the left side of the dam ($x < 50$ m), an initial water depth of 10 m was defined, and at the right side ($x > 50$ m), an initial water depth of 1 m was defined. The porosity increased linearly from 0 at $x = 0$ to 1 at $x = 100$ m. The domain was discretized, with a cell size of 0.1 m, and results are plotted for $t = 4$ s. A reference solution was calculated by solving a circular dam-break problem with a radius of 50 m and initial water depths of 10 m inside the dam and 1 m outside the dam (Guinot and Soares-Frazão, 2006).

In this test case, the porosity varied smoothly and the cell size was sufficiently small. Therefore, the conveyance porosity in the AP model was always very close to the storage porosity ($\psi/\phi \approx 1$), and the gradient of the porosity in the SP model was negligible. Thus, it is expected that both models behave similarly. Results for water depth and flow velocity are plotted in Fig. 2(a) and (b), respectively, and indeed it can be seen that the models converge to the reference solution in a very similar manner.

3.2. One-dimensional stationary flow with rapidly varying porosity

Initially presented in Sanders et al. (2008), this test case considered stationary flow in a one-dimensional channel in the face of a sudden porosity variation. The domain was 1000 m long and the porosity was defined as follows: $\phi = 1$ for $x < 400$ m and $x > 600$ m, $\phi = 0.75$ for $x > 410$ m and $x < 590$ m, ϕ decreased linearly from 1 to 0.75 between $x = 400$ m and 410 m, and ϕ increased linearly from 0.75 to 1 between $x = 590$ m and 600 m. The porosity function is plotted in Fig. 3. The domain was discretized, with a cell size of 0.25 m, and the model was run until a steady state was reached. A reference solution was obtained by solving the equivalent problem of a narrowing channel based on energy conservation (Bernoulli's law).

Results for water depth and flow velocity are plotted in Fig. 4(a) and (b), respectively. Both models behave similarly and converge to the steady-state solution, because, again, the variation of the porosity was smooth. Moreover, in the AP model, the conveyance porosity was close to the storage porosity, i.e., $\psi/\phi \approx 1$, and the gradient of the porosity in the SP model was negligible.

3.3. One-dimensional dam break with porosity discontinuity

This test case was initially presented in Guinot and Soares-Frazão (2006) and comprised a dam break with porosity discontinuity. The domain was 100 m long, with the dam positioned at $x = 50$ m, separating an initial water depth of 10 m and a porosity of 1 at the left side and an initial water depth of 1 m and a porosity of 0.1 at the right side of the dam. The domain was discretized, with the size of cells of 0.01 m. A reference solution was calculated by solving the Riemann problem with porosity suggested in Guinot and Soares-Frazão (2006), which yielded a nonlinear system of seven equations for seven unknowns that could be solved iteratively using, e.g., the Newton-Raphson procedure. The reference solution was thus based on the mathematical model of the SP model.

In this test case, the variation in the porosity had a sudden discontinuity. In the AP model, at the position of the discontinuity, the conveyance and storage porosities differed from each other significantly. In the SP model, the gradient of the porosity yielded a significant source term. Thus, a deviation in model results is expected. In Fig. 5, where model results are plotted against the reference solution at $t = 4$ s, it is observed that the results of the models deviate from each other. The results of the SP model are closer to the reference solution, while those of the AP model clearly deviate from it. Comparison with the reference solution shows that the shock position is inconsistent with the AP model, and the velocity and water depth of the AP model are overestimated downstream of the dam.

Here, it is noted that the AP model does not account for a porosity discontinuity across the cell edge in its mathematical model. The deviation in the results is therefore also due to a structural deviation between both models.

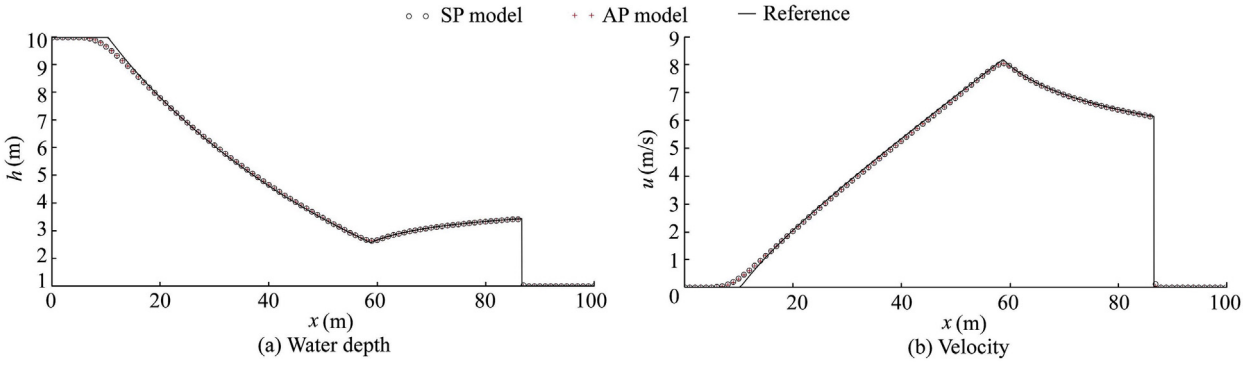

Fig. 2. Results of one-dimensional dam break of AP model and SP model with variable porosity at $t = 4$ s.

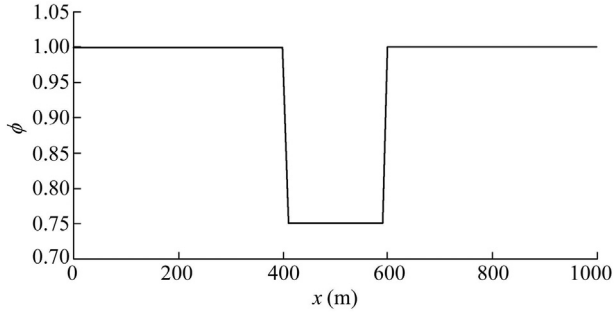

Fig. 3. Stationary flow with rapidly varying porosity in one-dimensional channel.

3.4. Discussion

The numerical test cases support the findings in Section 2, that in cases where the conveyance porosity differs significantly from the storage porosity, the AP model behaves differently from the SP model, and in cases where the conveyance porosity is close to the storage porosity, both models behave similarly.

In order to study this deviation in more detail, we consider the cell (without loss of generality) at the discontinuity ($x = 50.05$ m) in Section 3.3. At $t = 0$, at the cell edge located at the dam position, the following Riemann problem is solved with the SP model and the AP model, with the initial conditions as follows: $h_L = 10$ m, $h_R = 1$ m, $\phi_L = 1$, $\phi_R = 0.1$ ($\psi = 0.1$), and $\phi_L q_L = \phi_R q_R = 1$ m^2/s, where q_L and q_R are the unit-width discharges at the left and right sides of the cell edge, respectively. Calculating velocities at the cell edge, which will be the input of the Riemann solver for flux calculation, gives the following results of the SP model:

$$u_L = \frac{\phi_L q_L}{\phi_L h_L} = 0.1 \text{ m/s} \qquad u_R = \frac{\phi_R q_R}{\phi_R h_R} = 10 \text{ m/s} \tag{49}$$

and the following results of the AP model:

$$u_L = \frac{\phi_L q_L}{\psi h_L} = 1 \text{ m/s} \qquad u_R = \frac{\phi_R q_R}{\psi h_R} = 10 \text{ m/s} \tag{50}$$

which means that for different values of the conveyance porosity and storage porosity, different flow velocities are reconstructed at the cell edge, which in turn means that different Riemann problems are solved. Note that only the reconstructed velocities of the AP model and the BP model differ from each other, and the water depth at the cell center is used as the cell edge value in the AP model (Eq. (38)) as well as in the SP model.

It is easy to show that if the conveyance porosity equals the storage porosity, the AP model and SP model solve the same Riemann problem. Consider the Riemann problem with the following initial conditions: $h_L = 10$ m, $h_R = 1$ m, $\phi_L = 0.1$, $\phi_R = 0.1$ ($\psi = 0.1$), and $\phi_L q_L = \phi_R q_R = 1$ m^2/s. Now, reconstructed velocities used in the Riemann solver yield the same results of the SP and AP model: $u_L = 1$ m/s and

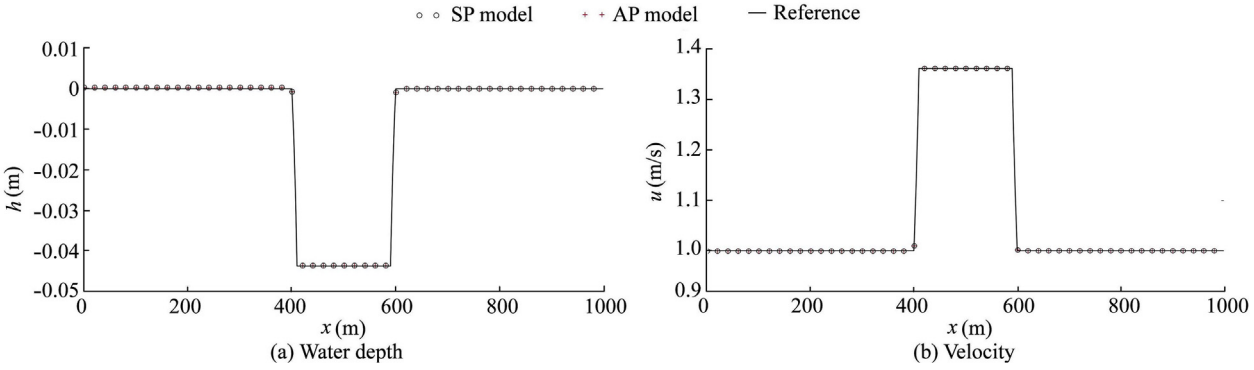

Fig. 4. Steady-state solutions of AP model and SP model with rapidly varying porosity.

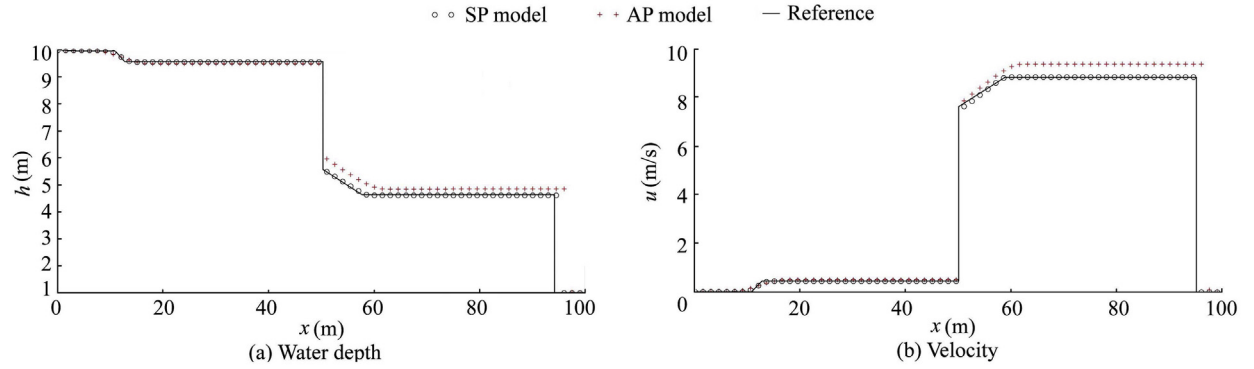

Fig. 5. Results of one-dimensional dam break of AP model and SP model with porosity discontinuity at t = 4 s.

$u_R = 10$ m/s. Thus, both models solve the same Riemann problem in this case.

In addition, in cases with a sudden porosity discontinuity, the geometric source term of the SP model becomes significant and enhances the SP model results, while the AP model does not account for this process.

3.5. Two-dimensional dam-break flow through idealized city

Both models were used to replicate a laboratory experiment conducted at the Université Catholique de Louvain, Belgium (Soares-Frazão and Zech, 2008). The computational domain is shown in Fig. 6. In the reservoir on the left side, an initial water level elevation of 0.40 m was defined. On the right side of the reservoir, an initial water level elevation of 0.011 m was set. A simplified building block was placed in the domain as sketched in Fig. 6, where individual houses are colored grey. The gate between both areas was opened at $t = 0$, inducing a dam-break flow. Measurement data for the water level elevation were available from gauges placed between and in front of the houses. The locations of some gauges used in the following analysis are shown in Fig. 7. The total simulation time was 15 s. Both models took about the same time to run the simulation with an average time step of 0.02 s.

Both the AP model and the SP model used structured meshes with a cell size of 0.25 m. The friction was accounted for by means of a Manning's coefficient of $n = 0.01$ s/m$^{1/3}$. In addition, a simple drag force closure was applied in both models, using a building drag coefficient of $c_D^b = 5$ m^{-2}. The storage porosity of the cells was deduced directly from the underlying buildings, i.e., the fraction of the cell occupied by a building was calculated individually in each cell. For the AP model, the conveyance porosity was calculated in the same way. No further calibration was carried out.

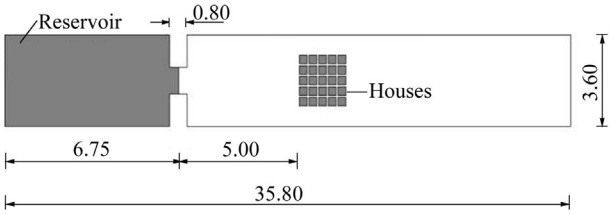

Fig. 6. Top view of computational domain with initial conditions (units: m).

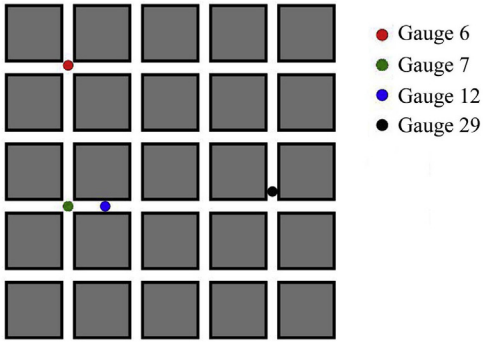

Fig. 7. Locations of some gauges.

Results at different gauges are compared in Fig. 8. In the two-dimensional test case, the models diverge significantly from one another. It is observed that the AP model shows better

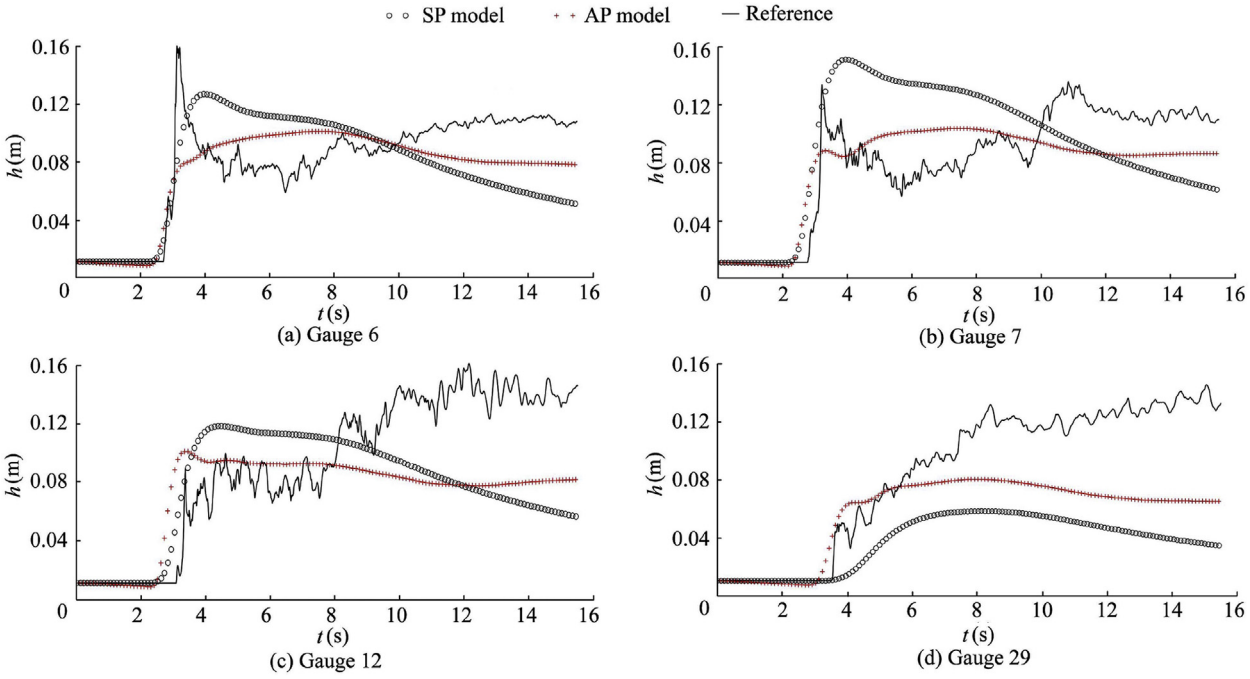

Fig. 8. Comparison of computed and measured water level elevations at different gauges.

agreement with measured data than the SP model. In the two-dimensional case, several factors lead to the difference in the model results. First, in cases with more complex geometry, the additional conveyance porosity of the AP model significantly enhances model results. The blocking and diversion of water due to the buildings can be represented more accurately with the addition porosity term. The large difference between results of the AP model and the SP model at gauge 29 can be explained as follows: when water arrives at this gauge, it has already traveled through almost the entire porous medium representing the building block, and water is not being blocked sufficiently at this gauge in the SP model. However, more water is diverted in the AP model due to its additional porosity term at the cell edges, causing large deviations between both model results. In addition, at the gauges located more toward the front, i.e., gauges 6, 7, and 12, it is observed that the models show greater agreement at the beginning of the simulation but diverge as time passes, with the SP model consistently showing more deviation from the measured data than the AP model.

The second reason for the deviation is related to the cell size of the computational mesh. In Soares-Frazão et al. (2008) and Velickovic et al. (2017), the resolution of the SP model was not designed to be as coarse as it was in this test case. For example, in Velickovic et al. (2017) the cell size was smaller than the building scale, and the porosity terms were usually used to further calibrate the model instead of using the layout of the building array to calculate the porosity terms (Soares-Frazão et al., 2008). Because neither of these strategies was used in the present case, the accuracy of the SP model was diminished. It can be concluded that, if the porosities are calculated based on the topography at the sub-grid scale, the AP model should be preferable.

4. Conclusions

A comparison between the SP model (Guinot and Soares-Frazão, 2006) and the AP model (Sanders et al., 2008) was presented.

The influence of the source term was analyzed using Roe-type approximate solutions that were initially presented in Murillo et al. (2007). It is seen that the ratio ψ/ϕ significantly influences the model behavior. If the ratio is close to 1, which implies smooth variation of porosity, similar behavior can be expected of both models, because the wave propagation speeds are similar and the geometric source term of the porosity gradient in the SP model is negligible. In addition, the analysis shows that the different source terms of the models yield different behaviors, depending on the configurations of porosities and water depths.

Computational test cases were carried out to further study the influence of the ratio ψ/ϕ on model results. Computational results support the conclusions of theoretical analysis. In cases with smooth porosity variation, the different model results converge toward each other while, in the face of sudden porosity changes, model results deviate.

It is emphasized that the deviation of the results of the AP model from the reference solution in the case of a one-dimensional dam break with porosity discontinuity does not have implications for the model quality. The reference solution has been derived by solving the Riemann problem for the SP model and it is therefore reasonable that the results of the SP model show better agreement with the reference solution in this test case.

The source terms in each model behave differently. The porosity gradient source term in the SP model accounts for spatial variations in porosity that drive water from regions with low porosity to regions with high porosity. Consequently, the influence of the source term is strong if the difference in porosities at both sides of the cell edge is large. In contrast, the source term in the AP model accounts for a pressure exchange at the interface between water and buildings, and it is not influenced by the difference in porosities at both sides of the cell edge. In the AP model a conveyance porosity is defined at the edge, i.e., the AP model has no mechanism to account for a porosity discontinuity. The source term in the AP model depends only on the water depth configuration at the edge.

A two-dimensional test case was presented to compare both models in a more complex setting. Model results significantly deviate from each other. The AP model shows better agreement with measured data. The conveyance porosity, which is absent from the SP model, significantly enhances the results of the AP model. It can be concluded that, if the porosities are calculated based on the topography at the sub-grid scale, the AP model is preferable.

References

Bird, R.B., Stewart, W.E., Lightfood, E.N., 2007. Transport Phenomena, second ed. John Wiley & Sons, New York.

Cunge, J.A., Holly, F.M., Verwey, A., 1980. Practical Aspects of Computational River Hydraulics. Pitman Advanced Publishing Program, London.

Defina, A., 2000. Two-dimensional shallow flow equations for partially dry areas. Water Resour. Res. 36(11), 3251−3264. https://doi.org/10.1029/2000WR900167.

Ferrari, A., Vacondio, R., Dazzi, S., Mignosa, P., 2017. A 1D-2D shallow water equations solver for discontinuous porosity field based on a generalized Riemann problem. Adv. Water Resour. 107, 233−249. https://doi.org/10.1016/j.advwatres.2017.06.023.

Guinot, V., Soares-Frazão, S., 2006. Flux and source term discretization in two-dimensional shallow water models with porosity on unstructured grids. Int. J. Numer. Meth. Fluid. 50(3), 309−345. https://doi.org/10.1002/fld.1059.

Guinot, V., 2012. Multiple porosity shallow water models for macroscopic modelling of urban floods. Adv. Water Resour. 37, 40−72. https://doi.org/10.1016/j.advwatres.2011.11.002.

Guinot, V., Sanders, B.F., Schubert, J.E., 2017. Dual integral porosity shallow water model for urban flood modelling. Adv. Water Resour. 103, 16−31. https://doi.org/10.1016/j.advwatres.2017.02.009.

Hinkelmann, R., 2005. Efficient Numerical Methods and Information-processing Techniques for Modeling Hydro- and Environmental Systems. Springer-Verlag, Berlin.

LeVeque, R.J., 2002. Finite Volume Methods for Hyperbolic Problems. Cambridge University Press, New York. https://doi.org/10.1017/CBO9780511791253.

Mohamed, K., 2014. A finite volume method for numerical simulation of shallow water models with porosity. Comput. Fluid 104, 9−19. https://doi.org/10.1016/j.compfluid.2014.07.020.

Murillo, J., García-Navarro, P., Burguete, J., Brufau, P., 2007. The influence of source terms on stability, accuracy and conservation in two-dimensional

shallow flow simulation using triangular finite volumes. Int. J. Numer. Meth. Fluid. 54(5), 543−590. https://doi.org/10.1002/fld.1417.

Nepf, H., 1999. Drag, turbulence, and diffusion in flow through emergent vegetation. Water Resour. Res. 35(2), 479−489. https://doi.org/10.1029/1998WR900069.

Özgen, I., Liang, D., Hinkelmann, R., 2016a. Shallow water equations with depth-dependent anisotropic porosity for subgrid-scale topography. Appl. Math. Model. 40(17−18), 7447−7473. https://doi.org/10.1016/j.apm.2015.12.012.

Özgen, I., Zhao, J., Liang, D., Hinkelmann, R., 2016b. Urban flood modeling using shallow water equations with depth-dependent anisotropic porosity. J. Hydrol. 541, 1165−1184. https://doi.org/10.1016/j.jhydrol.2016.08.025.

Roe, P.L., 1981. Approximate Riemann solver, parameter vectors, and difference schemes. J. Comput. Phys. 43(2), 357−372. https://doi.org/10.1016/0021-9991(81)90128-5.

Sanders, B.F., Schubert, J.E., Gallegos, H.A., 2008. Integral formulation of shallow-water equations with anisotropic porosity for urban flood modeling. J. Hydrol. 362(1−2), 19−38. https://doi.org/10.1016/j.jhydrol.2008.08.009.

Schubert, J.E., Sanders, B.F., 2012. Building treatments for urban flood inundation models and implications for predictive skill and modeling efficiency. Adv. Water Resour. 41, 49−64. https://doi.org/10.1016/j.advwatres.2012.02.012.

Soares-Frazão, S., Lhomme, J., Guinot, V., Zech, Y., 2008. Two-dimensional shallow-water model with porosity for urban flood modelling. J. Hydraul. Res. 46(1), 45−64. https://doi.org/10.1080/00221686.2008.9521842.

Soares-Frazão, S., Zech, Y., 2008. Dam-break flow through an idealised city. J. Hydraul. Res. 46(5), 648−658. https://doi.org/10.3826/jhr.2008.3164.

Velickovic, M., Zech, Y., Soares-Frazão, S., 2017. Steady-flow experiments in urban areas and anisotropic porosity model. J. Hydraul. Res. 55(1), 85−100. https://doi.org/10.1080/00221686.2016.1238013.